



This is a repository copy of *Effect of enhanced dissipation by shear flows on transient relaxation and probability density function in two dimensions*.

White Rose Research Online URL for this paper:
<http://eprints.whiterose.ac.uk/124630/>

Version: Published Version

Article:

Kim, E. and Movahedi, I. (2017) Effect of enhanced dissipation by shear flows on transient relaxation and probability density function in two dimensions. *Physics of Plasmas*, 24 (11). 112306. ISSN 1070-664X

<https://doi.org/10.1063/1.5003014>

Reuse

Items deposited in White Rose Research Online are protected by copyright, with all rights reserved unless indicated otherwise. They may be downloaded and/or printed for private study, or other acts as permitted by national copyright laws. The publisher or other rights holders may allow further reproduction and re-use of the full text version. This is indicated by the licence information on the White Rose Research Online record for the item.

Takedown

If you consider content in White Rose Research Online to be in breach of UK law, please notify us by emailing eprints@whiterose.ac.uk including the URL of the record and the reason for the withdrawal request.



eprints@whiterose.ac.uk
<https://eprints.whiterose.ac.uk/>

Effect of enhanced dissipation by shear flows on transient relaxation and probability density function in two dimensions

Eun-jin Kim, and Ismail Movahedi

Citation: [Physics of Plasmas](#) **24**, 112306 (2017);

View online: <https://doi.org/10.1063/1.5003014>

View Table of Contents: <http://aip.scitation.org/toc/php/24/11>

Published by the [American Institute of Physics](#)

**COMPLETELY
REDESIGNED!**



**PHYSICS
TODAY**

Physics Today Buyer's Guide
Search with a purpose.

Effect of enhanced dissipation by shear flows on transient relaxation and probability density function in two dimensions

Eun-jin Kim and Ismail Movahedi

School of Mathematics and Statistics, University of Sheffield, Sheffield S3 7RH, United Kingdom

(Received 1 September 2017; accepted 27 October 2017; published online 28 November 2017)

We report a non-perturbative study of the effects of shear flows on turbulence reduction in a decaying turbulence in two dimensions. By considering different initial power spectra and shear flows (zonal flows, streamers and zonal flows, and streamers combined), we demonstrate how shear flows rapidly generate small scales, leading to a fast damping of turbulence amplitude. In particular, a double exponential decrease in the turbulence amplitude is shown to occur due to an exponential increase in wavenumber. The scaling of the effective dissipation time scale τ_e , previously taken to be a hybrid time scale $\tau_e \propto \tau_\Omega^{2/3} \tau_\eta$, is shown to depend on types of shear flow as well as the initial power spectrum. Here, τ_Ω and τ_η are shearing and molecular diffusion times, respectively. Furthermore, we present time-dependent Probability Density Functions (PDFs) and discuss the effect of enhanced dissipation on PDFs and a dynamical time scale $\tau(t)$, which represents the time scale over which a system passes through statistically different states. *Published by AIP Publishing.* <https://doi.org/10.1063/1.5003014>

I. INTRODUCTION

Large scale shear flows are one of the most ubiquitous structures that naturally occur in a variety of physical systems and play an essential role in determining the overall transport in those systems. For example, stable shear flows can dramatically quench turbulent transport by shear-induced-enhanced-dissipation (see, e.g., Refs. 1–16). This occurs as a shear flow distorts fluid eddies, accelerates the formation of small scales, and dissipates them when a molecular diffusion becomes effective on small scales. One remarkable consequence of this turbulence quenching is the formation of transport barrier where the transport is dramatically reduced. The transition from low-confinement to high-confinement mode (L-H transition) in laboratory plasmas results from such formation of a transport barrier by shear flows (e.g., see Refs. 1, 2, 5, and 16), which is believed to be crucial for a successful operation of fusion devices. A similar transport barrier is also induced by a shear layer in the oceans¹⁸ and by an equatorial wind in the atmosphere.¹⁷ In the solar interior, a prominent large-scale shear flow due to the radial differential rotation was shown to lead to weak anisotropic turbulence and mixing in the tachocline^{7,8}—the boundary layer between the stable radiative interior and unstable convective layer. Our theoretical predictions have been confirmed by various numerical simulations (e.g., see Refs. 19 and 20).

The purpose of this paper is to investigate the effect of shear flows on the time-evolution of turbulence. In most of the previous works, the main focus was on the calculation of turbulent transport in a stationary state in a forced turbulence. Different models of turbulence such as 2D and 3D hydrodynamics and magnetohydrodynamic turbulence with/without rotation and stratification as well as different types of shear flows (e.g., linear, oscillatory, and stochastic shear flows)^{5–9} were considered previously. In comparison, much less work was done on the effect of shear flows on the

dynamics/time-evolution of turbulence, more precisely, how the enhanced/accelerated dissipation is manifested in time-evolution. A clear manifestation of shear flow effects on the dynamics seems especially important, given an ongoing controversy over the role of a shear flow in transport reduction, e.g., whether it is due to the reduction in cross phase (via an increased memory, as caused by waves) or the reduction in the amplitude of turbulence via enhanced dissipation (e.g., see Refs. 16 and 20 and references therein). A decaying turbulence provides us with an excellent framework in which this can be investigated in depth. We thus consider a simple decaying two-dimensional hydrodynamic turbulence model and examine the transient relaxation of the vorticity by different types of shear flows. We present time-dependent Probability Density Functions (PDFs) and discuss the effects of enhanced dissipation by shear flows on PDFs and effective dissipation time scale τ_e . We also introduce a dynamical time scale $\tau(t)$, which measures the rate of change in information associated with time-evolution; $1/\tau(t)$ represents the rate at which a system passes through statistically different states at time t (see Sec. III).

The simplicity of our model permits us to perform detailed analysis for different power spectra and shear flows. Nevertheless, our result that the dissipation and dynamical time scale depend on power spectrum and different types of shears is generic. The remainder of this paper is organised as follows: Section II introduces our model and highlights the importance of (i) a careful treatment of a diffusion term in a PDF method and (ii) a non-perturbative treatment of shear flows. Section III introduces dynamical time unit $\tau(t)$. Section IV discusses the effect of different shear flows on the evolution of Gaussian PDFs for different power spectra. Section V presents the analysis of one example of non-Gaussian PDFs. Discussion and Conclusions are found in Sec. VI. Appendixes contain some of the detailed mathematical derivations.

II. PROBABILITY DENSITY FUNCTION (PDF)

We consider the evolution equation for the fluctuating vorticity ω in two dimensions (2D). In the presence of a large-scale shear flow \mathbf{U} , turbulence becomes weak,^{6–9} and we can thus consider the following linear equation for fluctuating vorticity ω ($= -\nabla^2\phi$ where ϕ is a stream function, or electric potential in plasmas):

$$[\partial_t + \mathbf{U} \cdot \nabla]\omega = \nu \nabla^2 \omega. \quad (1)$$

For simplicity, Eq. (1) is taken to be dimensionless after appropriate rescaling of U , ω , ν , \mathbf{x} , and t . Note that since our main focus is on elucidating the effect of shear flows, scaling relations and relative values are of interest. Despite the fact that Eq. (1) is linear in ω , the equation for $p(\omega, \mathbf{x}, t)$ is not closed due to the dissipation term involving the second derivative. To show this, we express $p(\omega, \mathbf{x}, t)$ as the Fourier transform of the average of a generating function $Z = \exp(i\lambda\omega(\mathbf{x}, t))$ (e.g., see Refs. 21–23) as

$$\begin{aligned} p(\omega, \mathbf{x}, t) &= \langle \delta(\omega(\mathbf{x}, t) - \omega) \rangle = \frac{1}{2\pi} \left\langle \int d\lambda e^{-i\lambda(\omega - \omega(\mathbf{x}, t))} \right\rangle \\ &= \frac{1}{2\pi} \int d\lambda e^{-i\lambda\omega} \langle Z \rangle, \end{aligned} \quad (2)$$

where the angular brackets denote the average. By differentiating Z and using Eq. (1), we obtain

$$\partial_t Z = i\lambda(\partial_t \omega)Z = i\lambda[-\mathbf{U} \cdot \nabla \omega + \nu \nabla^2 \omega]Z. \quad (3)$$

By using $\partial_j Z = i\lambda(\partial_j \omega)Z$ and $\partial_{jj} Z = i\lambda(\partial_{jj} \omega)Z - \lambda^2 (\partial_j \omega)^2 Z$, we recast Eq. (3)

$$\begin{aligned} \partial_t Z + \mathbf{U} \cdot \nabla Z &= \nu \left[\partial_{jj} Z - \left[\partial_j (\ln Z)^2 \right] Z \right] \\ &= \nu \left[\nabla^2 Z + \lambda^2 (\partial_j \omega)^2 Z \right]. \end{aligned} \quad (4)$$

The second equation in Eq. (4) shows that the diffusion term gives rise to a nonlinear term in Z ($[\partial_j (\ln Z)^2]Z$). The Fourier transform of $\langle [\partial_j (\ln Z)^2]Z \rangle$ would then induce a convolution of $p(\omega, \mathbf{x}, t)$. On the other hand, the Fourier transform of $\langle \lambda^2 (\partial_j \omega)^2 Z \rangle$ in the last equation in Eq. (4) would require a conditional probability.²¹ For statistically independent $\partial_j \omega$ and Z , a linear equation can be written as

$$\partial_t p + \mathbf{U} \cdot \nabla p = \nu \nabla^2 p - \nu \langle (\partial_j \omega)^2 \rangle \partial_{\omega\omega} p. \quad (5)$$

For a homogeneous turbulence, $p(\omega, \mathbf{x}, t)$ becomes independent of \mathbf{x} , reducing Eq. (5) to

$$\partial_t p = -\nu \langle (\partial_j \omega)^2 \rangle \partial_{\omega\omega} p. \quad (6)$$

In general, the treatment of the diffusion term involving ν is tricky and has often been done approximately, or the diffusion term is simply neglected. Unfortunately, such an approximation cannot be justified in the presence of a shear flow as its effect is enhanced due to the accelerated formation of small scales, demanding the exact treatment of this diffusion term. For the same reason, the effect of \mathbf{U} cannot be treated perturbatively.

It is thus pivotal to solve Eq. (1) exactly in the Fourier space by using a time-dependent wave number. For example, let us consider a general type of a shear flow $\mathbf{U} = (U_s, U_z) = (-y\Omega_s, -x\Omega_z)$, where U_z and U_s are orthogonal flows, with their shearing rates Ω_z and Ω_s , respectively. We call U_z zonal flows (ZF) and U_s streamers in this paper. \mathbf{U} has the mean vorticity $\langle \omega_T \rangle = \nabla \times \mathbf{U} = (-\Omega_z + \Omega_s)\hat{z}$. In order to capture the effect of shear non-perturbatively, we use the following time-dependent wavenumber (e.g., see Refs. 6–9)

$$\omega(\mathbf{x}, t) = \tilde{\omega}(\mathbf{k}, t) \exp\{i(k_x(t)x + k_y(t)y)\}, \quad (7)$$

where $k_x(t)$ and $k_y(t)$ satisfy

$$\frac{dk_x(t)}{dt} = \Omega_z k_y, \quad \frac{dk_y(t)}{dt} = \Omega_z k_x. \quad (8)$$

Equations (7) and (8) give us a linear equation for the Fourier component $\tilde{\omega}(\mathbf{k}, t)$ as $\frac{\partial \tilde{\omega}(\mathbf{k}, t)}{\partial t} = -\nu[k_x(t)^2 + k_y(t)^2]\tilde{\omega}(\mathbf{k}, t)$ with the solution

$$\tilde{\omega}(\mathbf{k}, t) = \tilde{\omega}(\mathbf{k}(0), t=0) \exp\left(-\nu \int_0^t dt_1 [k_x(t_1)^2 + k_y(t_1)^2]\right). \quad (9)$$

Equation (9) would then permit us to compute $Z = \exp(i\lambda\omega(\mathbf{x}, t))$ and thus $p(\omega, \mathbf{x}, t)$ in Eq. (2). Once we have $p(\omega, \mathbf{x}, t)$, we can then find the equation for $p(\omega, \mathbf{x}, t)$.

III. DYNAMICAL TIME UNIT $\tau(t)$

Having introduced a time-dependent PDF in Sec. II, we now present how to utilize it to extract useful information diagnostics. A key characteristic of non-equilibrium processes is the variability in time (or in space), time-varying PDFs manifesting the change in information content in the system. We quantify the change in information by the rate at which a system passes through statistically different states.^{24–29} Mathematically, for a time-dependent PDF $p(x, t)$ for a stochastic variable x , we define the characteristic time-scale $\tau(t)$ over which $p(x, t)$ temporally changes *on average* at time t as follows:

$$\mathcal{E} \equiv \frac{1}{[\tau(t)]^2} = \int dx \frac{1}{p(x, t)} \left[\frac{\partial p(x, t)}{\partial t} \right]^2. \quad (10)$$

As defined in Eq. (10), $\tau(t)$ is a dynamical time unit, measuring the correlation time of $p(x, t)$. Alternatively, $1/\tau$ quantifies the (average) rate of change of information in time. A special case of $\tau(t) = \text{constant}$ is a geodesic where the information change is independent of time. Note that $\tau(t)$ in Eq. (10) is related to the second derivative of the relative entropy (or Kullback-Leibler divergence) (see Appendix A and Ref. 26) and that \mathcal{E} is the mean-square fluctuating energy for a Gaussian PDF (see Ref. 27).

The total change in information between the initial and final times, 0 and t , respectively, is then computed by the total elapsed time in units of $\tau(t)$ as $\mathcal{L}(t) = \int_0^t \frac{dt}{\tau(t)}$. \mathcal{L} (information length) provides the total number of different states that a system passes through from the initial state with the

PDF $p(x, t=0)$ at time $t=0$ to the final state with the PDF $p(x, t)$ at time t . For instance, in equilibrium, $\tau(t_1)$ is infinite so that measuring dt_1 in units of this infinite $\tau(t_1)$ at any t_1 gives $dt_1/\tau(t_1)=0$ and thus $\mathcal{L}(t)=0$, manifesting no flow of time in equilibrium. See [Appendix A](#) for the interpretation of \mathcal{L} from the perspective of the infinitesimal relative entropy. We note that ℓ [and thus $\tau(t)$] is based on Fisher information (cf. Ref. [30](#)) and is a generalisation of statistical distance^{31–33} to time-dependent problems.

As an example, let us consider the Gaussian PDF of the total vorticity $\omega_T = \langle \omega_T \rangle + \omega$ given by

$$p(\omega_T, \mathbf{x}, t) = \sqrt{\frac{\beta}{\pi}} \exp \left[-\beta(\omega_T - \langle \omega_T \rangle)^2 \right]. \quad (11)$$

Here, the angular brackets denote the average ($\langle \omega \rangle = 0$). $\beta = \frac{1}{2\langle \omega^2 \rangle}$ is the inverse temperature and $\beta \rightarrow \infty$ for a very narrow PDF. By using the property of the Gaussian distribution (e.g., $\langle \omega^4 \rangle = 3\langle \omega^2 \rangle^2$) (e.g., see Refs. [21](#) and [23](#)), we can show that \mathcal{E} in Eq. [\(10\)](#) is (see Refs. [26](#) and [28](#))

$$\mathcal{E}(t) = \frac{1}{\tau(t)^2} = \frac{1}{2} \frac{(\partial_t \beta)^2}{\beta^2} + 2\beta(\partial_t \langle \omega_T \rangle)^2. \quad (12)$$

The first term in Eq. [\(12\)](#) is due to the temporal change in PDF width ($\propto \beta^{-1/2}$), while the second is due to the change in the mean value measured in units of PDF width.

IV. GAUSSIAN PDFs

To gain a key insight, we start with the case where $\tilde{\omega}(\mathbf{k}(t=0))$ satisfies the Gaussian statistics. Using Eq. [\(9\)](#), we compute the average of the generating function $Z = \exp(i\lambda\omega(x, t))$ as follows:

$$\langle Z \rangle = \langle \exp(i\lambda\omega(x, t)) \rangle = \exp \left[-\frac{1}{2} \lambda^2 \langle \omega^2(\mathbf{x}, t) \rangle \right], \quad (13)$$

where

$$\langle \omega^2(\mathbf{x}, t) \rangle = \int d\mathbf{k}(t) d\mathbf{k}'(t) e^{i(\mathbf{k}(t)+\mathbf{k}'(t)) \cdot \mathbf{x}} \langle \tilde{\omega}(\mathbf{k}(t)) \tilde{\omega}(\mathbf{k}'(t)) \rangle. \quad (14)$$

Using Eq. [\(13\)](#) in Eq. [\(2\)](#) gives

$$p(\omega, \mathbf{x}, t) = \sqrt{\frac{\beta}{\pi}} \exp \left[-\beta\omega^2 \right]. \quad (15)$$

Here, $\beta = \frac{1}{2\langle \omega^2(\mathbf{x}, t) \rangle}$ is again the inverse temperature.

On the other hand, taking the time derivative Eq. [\(13\)](#) and Fourier transform gives

$$\partial_t p(\omega, \mathbf{x}, t) = \frac{1}{2} \frac{\partial^2}{\partial \omega^2} \left[[\partial_t \langle \omega^2(\mathbf{x}, t) \rangle] p(\omega, \mathbf{x}, t) \right], \quad (16)$$

consistent with Eq. [\(15\)](#).

In comparing the RHS of Eqs. [\(6\)](#) and [\(16\)](#), we have

$$\frac{1}{2} \partial_t \langle \omega^2(\mathbf{x}, t) \rangle = -\nu \langle (\partial_t \omega)^2 \rangle = \nu \langle \omega \nabla^2 \omega \rangle. \quad (17)$$

We will shortly show that Eq. [\(17\)](#) indeed holds for the Gaussian $\omega(\mathbf{x}, t)$ in a homogeneous turbulence. In the following, we analyse the zonal case in Sec. [IV A](#) and the combined shear flow cases $\Omega_z > 0$ and $\Omega_s > 0$ in Sec. [IV B](#), and $\Omega_z > 0$ and $\Omega_s < 0$ in Sec. [IV C](#).

A. ZF case: $\Omega_z > 0$ and $\Omega_s = 0$

For the case of zonal flow only (ZF), $\mathbf{U} = (0, -x\Omega_z)$, the mean vorticity $\langle \omega_T \rangle = -\Omega_z$, and the time dependent wave-number follows from Eq. [\(8\)](#) as

$$k_x(t) = k_x(0) + k_y \Omega_z t, \quad k_y(t) = k_y(0), \quad (18)$$

$$\begin{aligned} Q_1(t) &\equiv \int_0^t dt_1 |\mathbf{k}(t_1)|^2 \\ &= \frac{1}{3} (k_y \Omega_z)^2 t^3 + k_y k_x(0) \Omega_z t^2 + (k_x(0)^2 + k_y^2) t. \end{aligned} \quad (19)$$

With Eq. [\(19\)](#), Eq. [\(9\)](#) is rewritten as

$$\tilde{\omega}(k_x(t), k_y) = e^{-\nu Q_1(t)} \tilde{\omega}(k_x(0), k_y). \quad (20)$$

To compute the mean square of $\omega(\mathbf{x}, t)$ from Eq. [\(20\)](#), we assume a homogeneous turbulence at $t=0$ so that the translational invariance in space constrains the correlation function in the Fourier space as $\langle \tilde{\omega}(\mathbf{k}(0)) \tilde{\omega}(\mathbf{k}'(0)) \rangle = \delta(\mathbf{k}(0) + \mathbf{k}'(0)) \psi(\mathbf{k}(0))$, where $\psi(\mathbf{k}(0))$ is the initial power spectrum. Eq. [\(9\)](#) then gives us

$$\langle \tilde{\omega}(\mathbf{k}(t)) \tilde{\omega}(\mathbf{k}'(t)) \rangle = \delta(\mathbf{k}(0) + \mathbf{k}'(0)) \psi(\mathbf{k}(t)), \quad (21)$$

$$\psi(\mathbf{k}(t)) = e^{-2\nu Q_1(t)} \psi(\mathbf{k}(0)). \quad (22)$$

Using Eqs. [\(21\)](#) and [\(22\)](#) in [\(14\)](#), we then obtain

$$\langle \omega^2(\mathbf{x}, t) \rangle = \int d\mathbf{k} \psi(\mathbf{k}(t)). \quad (23)$$

We now confirm that Eq. [\(17\)](#) holds for Eqs. [\(22\)](#) and [\(23\)](#) since

$$\partial_t \langle \omega^2 \rangle = -2\nu \int d\mathbf{k} |\mathbf{k}(t)|^2 \psi(\mathbf{k}(t)),$$

$$\langle \omega \nabla^2 \omega \rangle = - \int d\mathbf{k} |\mathbf{k}(t)|^2 \psi(\mathbf{k}(t)). \quad (24)$$

In Secs. [IV A 1–IV A 3](#), we discuss PDFs and characteristic dissipation times scales by using different $\psi(\mathbf{k}(0))$.

1. δ -function power spectrum

The simplest case to consider is a δ -function power spectrum given by

$$\psi(\mathbf{k}(0)) = \delta(k_x(0) - a) \delta(k_y - b) \phi, \quad (25)$$

where ϕ is a constant. The power spectrum $\psi(\mathbf{k}(t))$ continues to have a δ -function with the peak at $k_x(t) = a + b\Omega_z t$ and $k_y(t) = b$ given by Eq. [\(18\)](#) with $k_x(0) = a$ and $k_y(0) = b$

$$\psi(\mathbf{k}(t)) = e^{-2\nu Q_1(t)} \delta(k_x(t) - a - b\Omega_z t) \delta(k_y(t) - b) \phi. \quad (26)$$

TABLE I. Scalings of τ_e and $\tau(t)$ for the initial δ -function and constant power spectra in the case of ZF with the shearing rate Ω_z and hyperbolic ZF+ST with the shearing rate $\Omega_z = \Omega_s = \Omega$. Gaussian power spectrum has the scaling between δ -function and constant power spectra.

Shear flows	ZF: Ω_z	ZF+ST: $\Omega_z = \Omega_s = \Omega$
δ -function	$\tau_e \propto \Omega_z^{-2/3}$	$\tau_e \propto \Omega^{-1} \ln \Omega$
Spectrum	$\tau(t) \propto t^{-1}$	$\tau(t) \propto e^{-\Omega t}$
Constant	$\tau_e \propto \Omega_z^{-1/2}$	$\tau_e \propto \Omega^{-1}$
Spectrum	$\tau(t) \propto t$	$\tau(t) \propto [\Omega \tanh(\Omega t)]^{-1}$

Using (23) and (26), we have

$$\langle \omega^2(\mathbf{x}, t) \rangle = \exp \left[-\frac{2\nu}{3} ((k_y \Omega_z)^2 t^3 + 3k_y \Omega_z t^2 k_x(0)) - 2\nu(k_x(0)^2 + k_y^2) t \right] \phi, \quad (27)$$

providing $\beta = \frac{1}{2\langle \omega^2(\mathbf{x}, t) \rangle}$ in Eq. (15).

For a strong shear $\Omega_z \gg \nu k_y^2$, the term $\frac{2\nu}{3} (k_y \Omega_z)^2 t^3$ in Eq. (27) causes the enhancement of dissipation over a usual exponential viscous damping $\exp(-2\nu(k_x(0)^2 + k_y^2)t)$. The effective dissipation time scale τ_e for such enhanced damping is found from $\frac{2\nu}{3} (k_y \Omega_z)^2 \tau_e^3 \sim 1$ as

$$\tau_e \sim \left(\nu k_y^2 \Omega_z^2 \right)^{-1/3} \equiv \left(\tau_\eta \tau_{\Omega_z}^2 \right)^{1/3}, \quad (28)$$

where $\tau_\eta = \frac{1}{\nu k_y^2}$ and $\tau_{\Omega_z} = \frac{1}{\Omega_z}$ are the viscous and shearing time scales, respectively. We now compare τ_e with the characteristic time scale $\tau(t) = \mathcal{E}^{-1/2}$ in Eq. (12) over which the information changes. From \mathcal{E} in Eq. (12), we have

$$\begin{aligned} \sqrt{2\mathcal{E}(t)} &= \nu |\mathbf{k}(t)|^2 \\ &= \nu \left(k_y^2 \Omega_z^2 t^2 + k_y k_x(0) \Omega_z t + k_x(0)^2 + k_y^2 \right). \end{aligned} \quad (29)$$

The time scale $\tau(t) = \mathcal{E}^{-1/2} \propto t^{-1}$ as $t \rightarrow \infty$ represents a very short dissipation time scale and enhanced dissipation due to the accelerated formation of small scales and their disruption. Clearly, unlike τ_e , $\tau(t)$ captures the dynamics of the systems, i.e., the dependence of the rate of dissipation on time. When $\Omega_z = 0$, $\tau(t) = \nu(k_x(0)^2 + k_y^2)$ in Eq. (29) becomes constant, which is the case of a geodesic (see Sec. III). The value of this constant $\tau(t)$ however depends on the initial wave number $\mathbf{k}(0)$, meaning that $\tau(t)$ is not scale invariant. This is to be contrasted to the case considered in Sec. IV B 2. Scalings of τ_e and $\tau(t)$ are summarized in Table I.

Figures 1(a) and 1(b) compare the time evolution of $p(\omega, t)$ for $\Omega_z = 2$ in (a) and for $\Omega_z = 0$ in (b) by using $k_y = 1$, $k_x(0) = 0$, $\phi = 1$, and $\nu = 0.1$. The initial PDF is shown in the bottom red curve and the time increases from the bottom to the top curve as $t = 0.6 \times n$, where $n = 0, 1, 2, 3, \dots, 10$. The narrowing of PDF width in time in Fig. 1(a) is in sharp contrast to a much smaller change in Fig. 1(b) between $t = 0$ and $t = 6$. A much faster narrowing in Fig. 1(a) manifests the enhanced dissipation of the mean square vorticity by Ω_z .

2. Constant power spectrum

$\tau_e \propto \Omega_z^{-2/3}$ in Eq. (28) is specific to the case of the δ -function power spectrum where there is unique wavenumber at $t = 0$ that evolves according to Eq. (18). To understand how τ_e is affected in the presence of different $\mathbf{k}(0)$ modes, we consider a constant spectrum by taking $\psi = \text{constant} = \phi$. Then, the power spectrum evolves in time as follows:

$$\psi(\mathbf{k}(t), t) = e^{-2\nu Q_1(t)} \phi, \quad (30)$$

where $Q_1(t)$ is given in Eq. (19). From Eqs. (23) and (30), we obtain

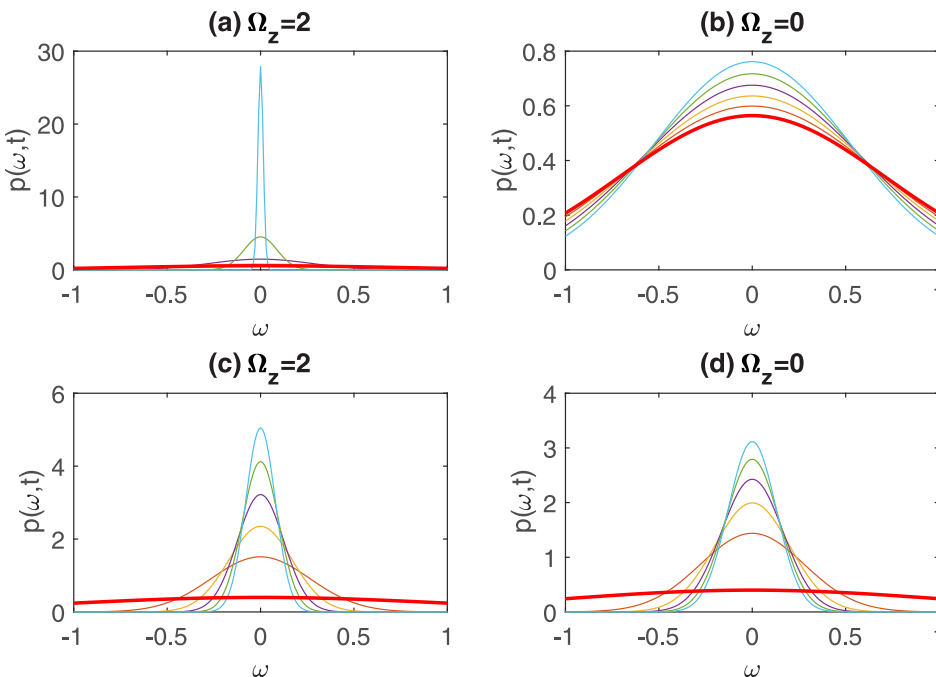


FIG. 1. Time evolution of $p(\omega, t)$ in panels (a) and (b) for the δ -function power spectrum in (25) and in panels (c) and (d) for the Gaussian power spectrum in Eq. (A1); $t = 0.6 \times n$ where $n = 0, 1, 2, 3, \dots, 10$ increases from the bottom to the top curves. The bottom red curve is for the initial PDF. $\alpha = 100$, $\nu = 0.1$, $k_x(0) = 0$, $k_y = 1$, and $\phi = 1$.

$$\langle \omega^2(x, t) \rangle = \frac{\pi}{2\nu t \sqrt{4 + \frac{1}{3}\Omega_z^2 t^2}} \phi \quad (31)$$

after performing the Gaussian integrals over k_y and $k_x(0)$. Equation (31) shows that Ω_z changes the scaling of $\langle \omega^2(x, t) \rangle$ from t^{-1} to t^{-2} by the enhanced dissipation. In this case, τ_e is found from $\nu\Omega_z\tau_e^2 \sim 1$ as

$$\tau_e \propto (\Omega_z\nu)^{-\frac{1}{2}}. \quad (32)$$

Thus, the dependence of $\tau_e \propto \Omega_z^{-1/2}$ on Ω_z is weaker than $\tau_e \propto \Omega_z^{-2/3}$ for a δ -function spectrum as the effect of shearing is reduced in the case of multiple modes. This is basically because the distortion of an eddy by shearing follows a wave number specific time evolution [e.g., Eq. (18)]; the effect of a shear on multiple modes is not coherent as eddies with different wave numbers evolve differently and is thus less effective.

This reduced shearing effect can also be inferred from \mathcal{E} in Eq. (12), which becomes

$$\mathcal{E}(t) = \frac{\left(4 + \frac{2}{3}\Omega_z t^2\right)^2}{2t^2 \left(4 + \frac{1}{3}\Omega_z t^2\right)^2}. \quad (33)$$

Thus, Eq. (33) gives the time scale $\tau(t) = \mathcal{E}^{-1/2} \propto t$ for $\Omega_z t \gg 1$. This should be compared with $\tau(t) \propto t^{-1}$ in the case of a δ -function power spectrum above (see Table I). The increase of $\tau(t)$ with t means a longer time scale of dissipation and thus it manifests that the dissipation becomes less effective for large time. Similar results are shown for the case of an anisotropic power spectrum with $k_x(0)=0$ in Appendix B. We note that the mean square vorticity in Eq. (31) apparently diverges at $t=0$ due to the unlimited range

of the \mathbf{k} integral for an initial constant power spectrum. Mathematically, this problem is readily ratified by using a localised spectrum in Sec. IV A 3.

3. Gaussian power spectrum

The initial Gaussian power spectrum $\psi(0) = \frac{1}{\alpha\pi} e^{-\frac{1}{2}(k_x(0)^2 + k_y^2)} \phi$ gives

$$\psi(\mathbf{k}(t)) = \frac{1}{\alpha\pi} e^{-\frac{1}{2}(k_x(0)^2 + k_y^2) - 2\nu Q_1(t)} \phi, \quad (34)$$

where $Q_1(t)$ is given in Eq. (19); α represents the width of the initial power spectrum; $\alpha \rightarrow 0$ and $\alpha \rightarrow \infty$ recover the δ -function and constant power spectrum, respectively. To understand the effect of Ω_z on the evolution of $\psi(\mathbf{k}(t))$ in (34), we use $k_x(0) = k_x(t) - \Omega_z k_y t$ and present $\psi(\mathbf{k}(t))$ in Fig. 2. Without diffusion ($\nu=0$), $\psi(\mathbf{k}(t))$ in Fig. 2(a) shows the generation of large k_x wave number due to ZF shearing. When a diffusion ($\nu=0.1$) is included in Fig. 2(b), large k_x (and k_y) modes quickly damp due to molecular dissipation, $\psi(\mathbf{k}(t))$ forming a sharp peak around $k_x = k_y = 0$.

On the other hand, using Eqs. (34) and (19) in (23), we find

$$\langle \omega^2(x, t) \rangle = \frac{1}{\alpha} \sqrt{\frac{1}{A}} \phi, \quad (35)$$

where $A = (2\nu t + \alpha^{-1})^2 + \frac{1}{3}(\nu t)(\Omega_z t)^2[\nu t + 2\alpha^{-1}]$. We note that in the limit of $t \rightarrow 0$ and $t \rightarrow \infty$, Eq. (A1) is reduced to

$$\langle \omega^2(x, t) \rangle_{t \rightarrow 0} \rightarrow \phi, \quad \langle \omega^2(x, t) \rangle_{t \rightarrow \infty} \rightarrow \frac{\sqrt{3}}{\alpha\nu\Omega_z t^2} \phi, \quad (36)$$

respectively. The second equation in Eq. (36) recovers the limit of a δ -function power spectrum in Eq. (31) (up to an unimportant small numerical factor). Eq. (35) very

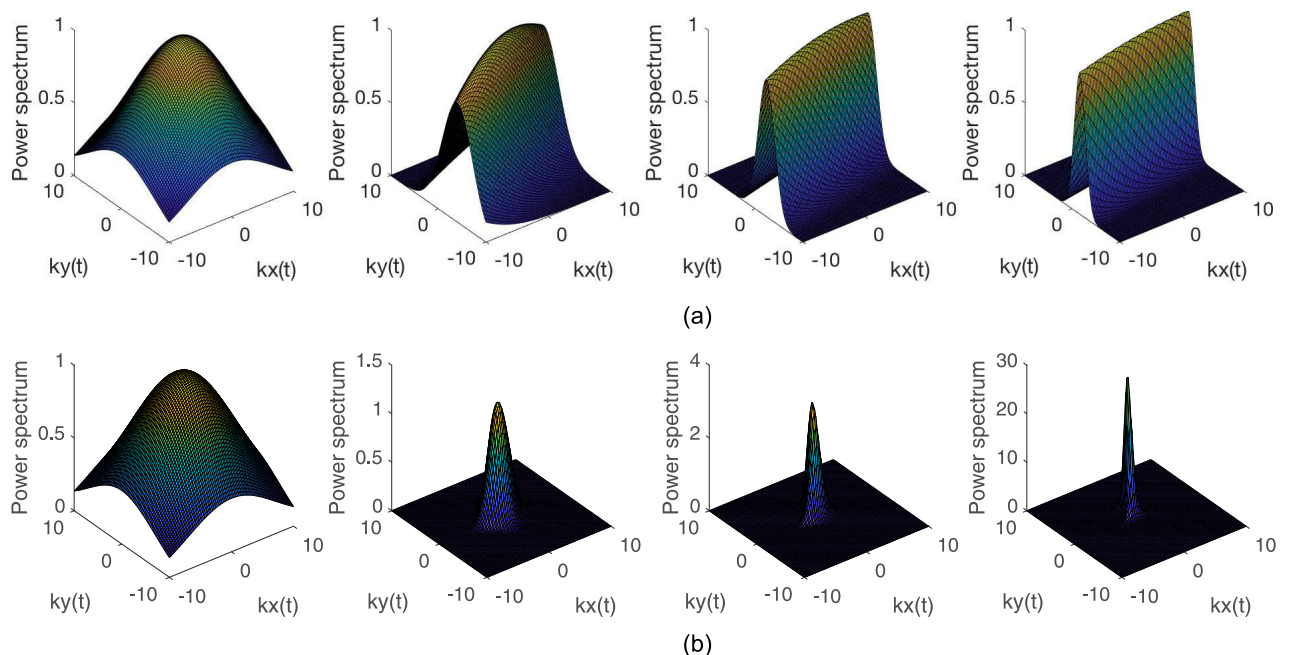


FIG. 2. (a) Time evolution of power spectrum ($t=0, 1, 2, 3$ increasing from left to right) for $\Omega_z=2$, $\Omega_s=0$, $\alpha=100$, $\phi=1$, and $\nu=0$. (b) The same as (a) but for $\nu=0.1$.

conveniently shows the transition of the scaling of τ_e from $\propto \Omega_z^{-2/3}$ in Eq. (28) to $\propto \Omega_z^{-1/2}$ in Eq. (32) as α increases (see also above).

Figures 1(c) and 1(d) show the evolution of $p(\omega, t)$ for this Gaussian power spectrum for $\Omega_z = 2$ and $\Omega_z = 0$, respectively. Here, parameter values are the same as those in Figs. 1(a) and 1(b) apart from $\alpha = 100$. Comparing Fig. 1(c) with Fig. 1(a), we see much slower narrowing of the PDFs as the shearing effect is less effective in the presence of multiple \mathbf{k} modes. As observed in Figs. 1(a) and 1(b), the PDF in Fig. 1(d) for $\Omega_z = 0$ narrows slower than that in Fig. 1(c). However, comparing Figs. 1(b) and 1(d), the presence of multiple \mathbf{k} modes tends to promote dissipation (due to high wave number modes).

B. Hyperbolic ZF+ST case: $\Omega_z > 0$ and $\Omega_s > 0$

Compared with the case of zonal flows, the combined effect of Zonal Flows and STreamers (ZF+ST) has been studied much less. We show below that the action of ZF+ST can lead to an exponentially fast formation of small scale structure. For $\mathbf{U} = (-y\Omega_s, -x\Omega_z)$ with $\Omega_s > 0$ and $\Omega_z > 0$, \mathbf{U} has the mean vorticity $\nabla \times \mathbf{U} = (-\Omega_z + \Omega_s)\hat{z}$, which becomes zero for $\Omega_z = \Omega_s$. The solution to Eq. (18) can be found as

$$k_y(t) = \bar{k} \frac{\Omega}{\Omega_z} \cosh(\Omega t + \theta), \quad k_x(t) = \bar{k} \sinh(\Omega t + \theta), \quad (37)$$

where

$$\Omega = \sqrt{\Omega_z \Omega_s}, \quad \bar{k} \left[k_y(0)^2 + k_x(0)^2 \frac{\Omega^2}{\Omega_z^2} \right]^{\frac{1}{2}}, \quad (38)$$

$$\sinh(\theta) = \frac{k_x(0)}{\bar{k}}, \quad \cosh \theta = \frac{\Omega_z k_y(0)}{\Omega \bar{k}}. \quad (39)$$

We focus on the case of $\Omega_z = \Omega_s = \Omega$ with zero mean vorticity, in which case $k_x^2 + k_y^2 = \bar{k}^2 \cosh[2(\Omega t + \theta)]$ follows from Eq. (37). Thus, with the help of Eqs. (38) and (39), we obtain $Q_2(t) = \int_0^t dt_1 |\mathbf{k}(t_1)|^2$ as

$$Q_2(t) = \frac{1}{4\Omega} [(k_x(0) + k_y(0))^2 (e^{2\Omega t} - 1) + (k_x(0) - k_y(0))^2 (1 - e^{-2\Omega t})]. \quad (40)$$

Since $\mathbf{k}(t)$ starting with $\mathbf{k}(0)$ changes in time according to Eq. (37), in order to see how the power spectrum evolves in time, we need to express $Q_2(t)$ in Eq. (40) in terms of $\mathbf{k}(t)$. To this end, we solve Eq. (37) for $k_x(0)$ and $k_y(0)$ to find $k_y(0) = k_y(t) \cosh(\Omega t) - k_x(t) \sinh(\Omega t)$ and $k_x(0) = k_x(t) \cosh(\Omega t) - k_y(t) \sinh(\Omega t)$, and thus

$$\begin{aligned} k_x(0) + k_y(0) &= [k_x(t) + k_y(t)] e^{-\Omega t}, \\ k_x(0) - k_y(0) &= [k_x(t) - k_y(t)] e^{\Omega t}. \end{aligned} \quad (41)$$

By using Eq. (41) in Eq. (40), we have

$$Q_2(t) = \frac{1}{4\Omega} [(k_x(t) + k_y(t))^2 (1 - e^{-2\Omega t}) + [k_x(t) - k_y(t)]^2 (e^{2\Omega t} - 1)]. \quad (42)$$

Interestingly, Eq. (42) shows that the dissipation $Q_2(t)$ takes its minimum value when $k_x(t) = k_y(t)$. Furthermore, from Eq. (41), we also find

$$\begin{aligned} k_x(0)^2 + k_y(0)^2 &= \frac{1}{2} [(k_x(t) - k_y(t))^2 e^{2\Omega t} \\ &+ (k_x(t) + k_y(t))^2 e^{-2\Omega t}], \end{aligned} \quad (43)$$

which also takes its minimum along $k_x(t) = k_y(t)$. The minimum of Eqs. (42) and (43) along $k_x(t) = k_y(t)$ is later shown to give a peak in the power spectrum $\psi(\mathbf{k}(t))$ in Sec. V (see Fig. 3). We refer to $k_x(t) = k_y(t)$ as the principle direction in the following.

1. δ -function power spectrum

For a δ -function power spectrum given by Eq. (25), the power spectrum $\psi(\mathbf{k}(t))$ continues to have a δ -function with the peak at $k_x(t)$ and $k_y(t)$ given by Eq. (37) with $k_x(0) = a$ and $k_y(0) = b$. This leads to

$$\begin{aligned} \langle \omega^2(\mathbf{x}, t) \rangle &= \exp \left[-\frac{\nu}{2\Omega} [(k_x(0) + k_y(0))^2 (e^{2\Omega t} - 1) \right. \\ &\left. - (k_x(0) - k_y(0))^2 (e^{-2\Omega t} - 1)] \right] \phi. \end{aligned} \quad (44)$$

From Eq. (44), we find the effective diffusion time τ_e

$$\tau_e \sim \frac{1}{2\Omega} \ln \left(\frac{2\Omega}{\nu |\mathbf{k}_0|^2} \right). \quad (45)$$

τ_e in Eq. (45) is smaller than Eq. (28) for a sufficiently large Ω , with a stronger dependence $\Omega^{-1} \ln \Omega$ on Ω , in comparison with $\Omega_z^{-2/3}$ in ZF case. Furthermore, due to the double exponential decrease in $\langle \omega^2 \rangle$, $\tau(t)$ in Eq. (12) is reduced exponentially fast as

$$\tau(t) \propto e^{-\Omega t}. \quad (46)$$

The exponentially decreasing $\tau(t)$ in Eq. (46) reflects a very efficient dissipation by ZF+ST. The evolution of PDF is shown in Fig. 3 for $\Omega = 2$ in (a) and $\Omega = 0$ in (b). The time $t = 0.2 \times n$, where $n = 0, 1, 2, 3, 4$, and 5 increases from the bottom to the top curves. The bottom red curve is for the initial PDF. Comparing Fig. 3(a) with Fig. 1(a), we see a much faster narrowing of the PDFs in the hyperbolic ZF+ST case due to a much faster dissipation. (Note that the total time span $t = [0, 1]$ in Fig. 3 is much smaller than $t = [0, 6]$ in Fig. 1.) The change in Fig. 3(b) with $\Omega = 0$ is too small to be seen.

2. Constant power spectrum

For an initial constant power spectrum $\psi(0) = \phi$, the power spectrum again evolves as $\psi(\mathbf{k}(t), t) = e^{-2\nu Q_2(t)} \phi$, where Q_2 is given in Eq. (40). Therefore, by using Eqs. (23) and (40), we find

$$\begin{aligned} \langle \omega^2(x, t) \rangle &= \frac{1}{2} \int dpdq \exp \\ &\times \left[-\frac{\nu}{2\Omega} [p^2 (e^{2\Omega t} - 1) + q^2 (1 - e^{-2\Omega t})] \right] \phi \\ &= \frac{\Omega \phi}{2\pi \nu \sinh(\Omega t)}. \end{aligned} \quad (47)$$

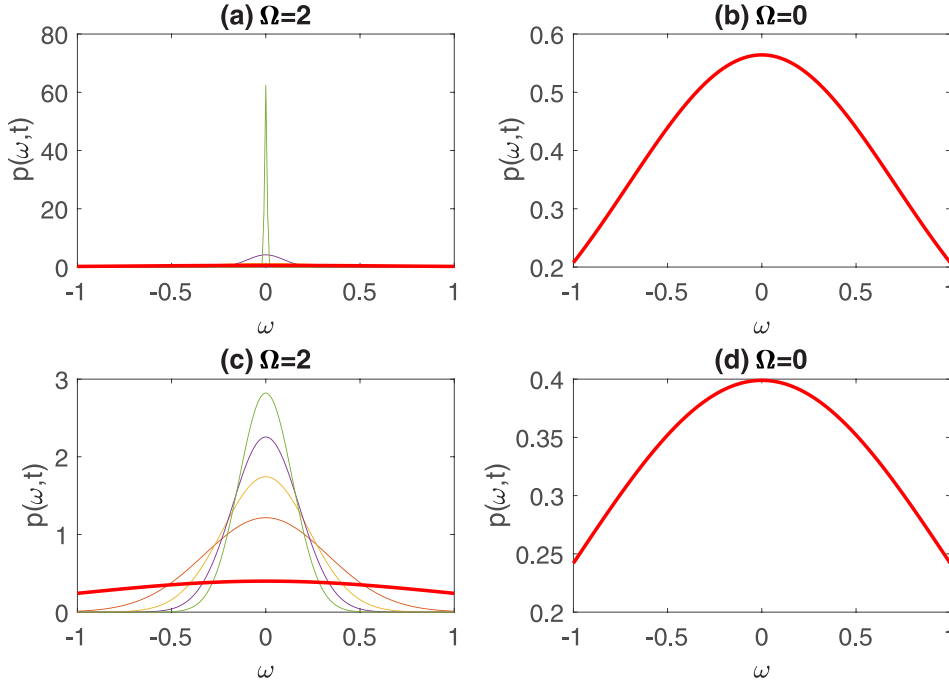


FIG. 3. Time evolution of $p(\omega, t)$ for the δ -function power spectrum in Eq. (44) in panels (a) and (b) and for the Gaussian power spectrum in Eq. (51) in panels (c)–(d); $t = 0.2 \times n$, where $n = 0, 1, 2, 3, 4, 5$ increases from the bottom to the top curves. The bottom red curve is for the initial PDF. $\alpha = 100$, $\nu = 0.1$, and $\phi = 1$.

Here, we performed the integrals over $p \equiv k_x(0) + k_y(0)$ and $q \equiv k_x(0) - k_y(0)$.

Compared with the δ -function power spectrum, the effect of shear flow is reduced from double exponential to exponential. For $\Omega t \gg 1$, $\langle \omega^2(x, t) \rangle \sim \frac{\Omega}{2\nu} e^{-\Omega t} \phi$, giving an effective diffusion time

$$\tau_e \sim \Omega^{-1}. \quad (48)$$

Interestingly, $\tau(t)$ in this case has a similar dependence on Ω since

$$\tau(t) = \frac{1}{\Omega \tanh(\Omega t)}, \quad (49)$$

approaching a constant value Ω^{-1} (!) for $t \gg \Omega^{-1}$. This is another example of a geodesic, which is more interesting than the case of $\Omega_z = 0$ in Eq. (29) because Eq. (49) is induced by non-zero Ω in the presence of different $\mathbf{k}(t)$ modes which evolve from an initial constant power spectrum. In fact, $\tau(t) \sim \Omega^{-1}$ explicitly shows that Ω is the very cause of information change. On the other hand, in comparison with the exponentially decreasing $\tau(t)$ in Eq. (46), Eq. (49) again illustrates the reduced shearing effect due to the presence of multiple \mathbf{k} modes. Finally, we note that the divergence at $t = 0$ is due to the unbounded power spectrum as in the case of Eq. (31). Scalings of τ_e and $\tau(t)$ are summarized in Table I.

3. Gaussian power spectrum

For $\psi(0) = \frac{1}{\alpha\pi} e^{-\frac{1}{\alpha}(k_x(0)^2 + k_y(0)^2)} \phi$, we have

$$\psi(\mathbf{k}(t)) = \frac{1}{\alpha\pi} e^{-\frac{1}{\alpha}(k_x(0)^2 + k_y(0)^2) - 2\nu Q_2(t)} \phi, \quad (50)$$

where Q_2 is given by Eq. (40). By using Eqs. (42) and (43) in Eq. (50), we present the evolution of the power spectrum

$\psi(\mathbf{k}(t))$ in Fig. 4 for $\Omega = 2$, where time increases from left to right as $t = 0, 0.6, 1.2$, and 1.8 . Without diffusion ($\nu = 0$), $\psi(\mathbf{k}(t))$ in Fig. 4(a) shows a fast reduction in $\psi(\mathbf{k}(t))$ along $k_x(t) + k_y(t) = 0$, with the peak forming along the principle direction $k_x(t) = k_y(t)$. When diffusion ($\nu = 0.1$) is included in Fig. 4(b), modes of large wavenumber also damp along the principle direction in time due to the molecular dissipation although the damping is weaker compared to that along $k_x(t) + k_y(t) = 0$. This is because the dissipation $Q_2(t)$ in Eq. (42) and $k_x(0)^2 + k_y(0)^2$ in Eq. (43) are minimized along $k_x(t) = k_y(t)$, as noted previously.

Now, Eq. (50) leads to the mean square vorticity

$$\begin{aligned} \langle \omega^2(x, t) \rangle &= \frac{2}{\alpha\pi} \int dpdq \exp \left[-\frac{\nu}{2\Omega} \left[p^2 (e^{2\Omega t} - 1) \right. \right. \\ &\quad \left. \left. + q^2 (1 - e^{-2\Omega t}) - \frac{1}{\alpha} (p^2 + q^2) \right] \right] \phi \\ &= \frac{2}{\alpha\sqrt{AB}}, \end{aligned} \quad (51)$$

where

$$A = \frac{\nu}{2\Omega} (e^{2\Omega t} - 1) + \frac{1}{\alpha}, \quad B = \frac{\nu}{2\Omega} (1 - e^{-2\Omega t}) + \frac{1}{\alpha}. \quad (52)$$

$\tau_e \propto \Omega^{-1}$ is thus similar to Eq. (48) for $t \gg \Omega^{-1}$. However, in contrast to Eq. (49), $\tau(t)$ becomes constant for $t \gg \Omega^{-1}$ only for a sufficiently large α , that is, in the limit of a constant power spectrum. Figure 3(c) shows the evolution of $p(\omega, t)$ for this case using the same parameter values $\Omega_z = \Omega_s = \Omega = 2$ as in Fig. 3(a) apart from $\alpha = 100$. Comparing Fig. 3(c) with Fig. 3(a), we see much slower narrowing of the PDFs as the shearing effect is less effective in the presence of multiple \mathbf{k} modes, as observed in Fig. 1. The evolution of $p(\omega, t)$ for $\Omega = 0$ is shown in Fig. 3(d), which hardly changes.

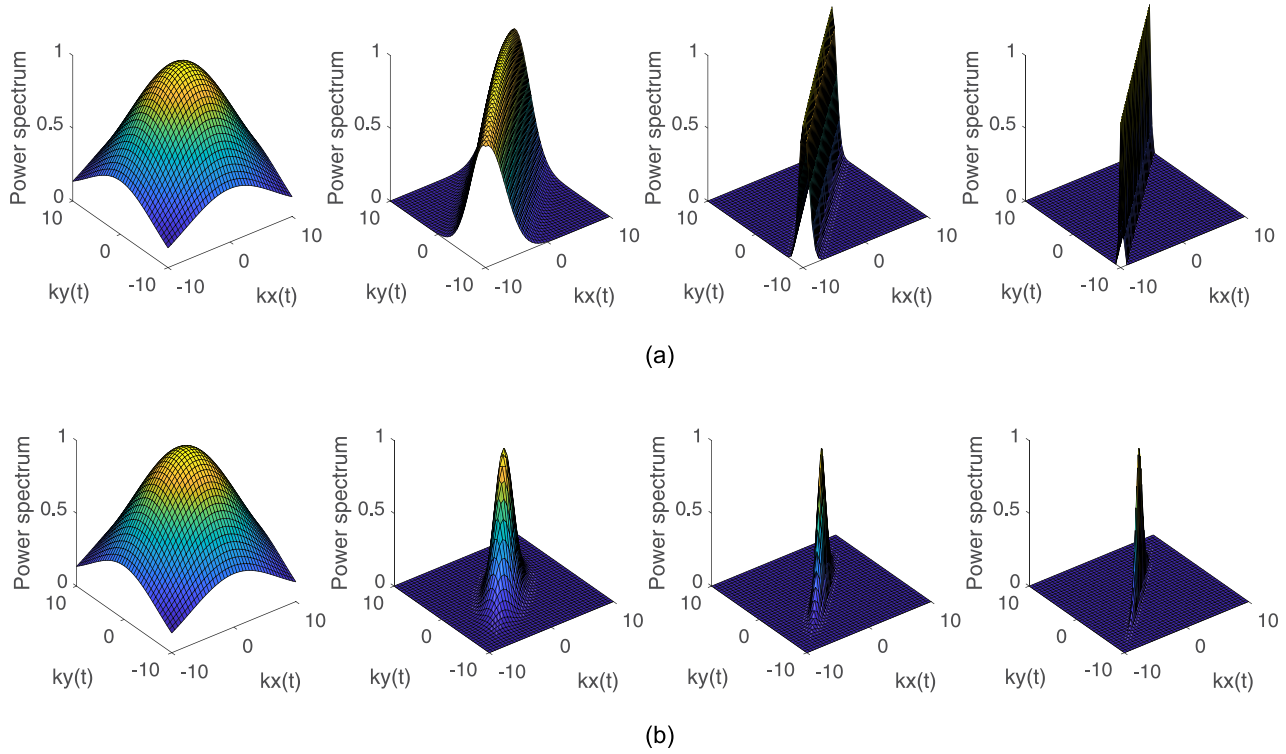


FIG. 4. (a) Time evolution of power spectrum ($t=0, 0.6, 1.2, 1.8$ increasing from left to right) for $\Omega_z = \Omega_x = \Omega_y = 2$, $\alpha = 100$, $\phi = 1$, and $\nu = 0$. (b) The same as (a) but for $\nu = 0.1$.

C. Elliptic ZF+ST case

For the hyperbolic ZF+ST case in Sec. IV B, the sign of zonal flow and streamer shear is the same. When they have different signs, ZF+ST leads to a rotating wave number. To see this, we consider $\mathbf{U} = (y\Omega_y, -x\Omega_x)$ with $\Omega_y > 0$ and $\Omega_x > 0$ which has the nonzero mean vorticity $\nabla \times \mathbf{U} = -(\Omega_x + \Omega_y)\hat{z}$. For this ZF+ST, we find the solution to Eq. (18) as $k_y(t) = \bar{k} \frac{\Omega}{\Omega_z} \cos(\Omega t + \theta)$ and $k_x(t) = \bar{k} \sin(\Omega t + \theta)$, where $\Omega = \sqrt{\Omega_x \Omega_y}$, $\bar{k} = [k_x(0)^2 + k_y(0)^2 \frac{\Omega_z^2}{\Omega^2}]^{1/2}$, and $\sin(\theta) = \frac{k_x(0)}{\bar{k}}$, $\cos(\theta) = \frac{\Omega_z k_y(0)}{\Omega \bar{k}}$. When $\Omega_z = \Omega_x = \Omega_y$, $k_x^2 + k_y^2 = k_x(0)^2 + k_y(0)^2$ is a constant in time, with no enhancement of dissipation. However, for $\Omega_z \neq \Omega_x, \Omega_y$, $k_x^2 + k_y^2 = \bar{k}^2 [\sin^2(\Omega t + \theta) + \frac{\Omega_z^2}{\Omega^2} \cos^2(\Omega t + \theta)]$. Although the overall dissipation may not be significantly enhanced by this shear flow, there is an interesting effect on the dynamics due to oscillatory dissipation, k_x or k_y , which provides a periodic background (or potential). This is discussed in our accompanying paper.³⁴

V. NON-GAUSSIAN PDFs

In Sec. IV, we investigated the effect of shear flows on the evolution of the Gaussian PDFs and power spectra. The main effect was the shift of power to larger wavenumber, accelerating dissipation, and narrowing PDF width. We now extend our study to a non-Gaussian case to examine the effect of shear flows on the form of PDF. Although there are many possible causes for non-Gaussian PDFs, we consider one example of an inhomogeneous turbulence. That is, we drop the assumption of homogeneous turbulence and instead prescribe the profile of the initial vorticity fluctuation as

$$\begin{aligned} \tilde{\omega}(\mathbf{k}(0), t = 0) &= \frac{1}{\alpha\pi} e^{-\frac{1}{2\alpha}(k_x(0)^2 + k_y(0)^2)}, \\ \omega(\mathbf{x}, t = 0) &= e^{-\frac{\alpha}{2}(x^2 + y^2)}, \end{aligned} \tag{53}$$

where α is a positive random variable. Note that when $\alpha = 0$, Eq. (53) gives a constant $\omega(\mathbf{x}, 0)$ while the nonzero constant $\alpha (> 0)$ gives the typical length scale l of the profile of the initial vorticity fluctuation as $l \sim \alpha^{-1/2}$. A random positive α makes the profile of the initial vorticity fluctuation on different length scales. By considering the hyperbolic shear flow considered in Sec. IV B, we have

$$\tilde{\omega}(\mathbf{k}(t), t) = \frac{1}{\alpha\pi} e^{-\frac{1}{2\alpha}(k_x(0)^2 + k_y(0)^2) - \nu Q_2(t)}, \tag{54}$$

where $Q_2(t)$ is given in Eq. (40). In order to take the inverse Fourier transform of Eq. (54) to find $\omega(\mathbf{x}, t)$, we first write Eq. (37) in terms of $p = k_x(0) + k_y(0)$ and $q = -k_x(0) + k_y(0)$ as $k_y(t) = \frac{1}{2}[pe^{\Omega t} + qe^{-\Omega t}]$ and $k_x(t) = \frac{1}{2}[pe^{\Omega t} - qe^{-\Omega t}]$ so that

$$\mathbf{k}(t) \cdot \mathbf{x} = \frac{1}{2} [pe^{\Omega t} z_1 + qe^{-\Omega t} z_2], \tag{55}$$

where

$$z_1 = x + y, \quad z_2 = y - x. \tag{56}$$

Then, by using Eqs. (40), (54), and (55), we obtain $\omega(\mathbf{x}, t) = \int d\mathbf{k}(t) e^{i\mathbf{k}(t) \cdot \mathbf{x}} \tilde{\omega}(\mathbf{k}(t), t)$ as

$$\omega(\mathbf{x}, t) = \frac{1}{2\alpha\sqrt{CD}} \exp \left[-\frac{e^{2\Omega t} z_1^2}{8C} - \frac{e^{-2\Omega t} z_2^2}{8D} \right]. \tag{57}$$

Here

$$C = \frac{\nu}{4\Omega}(e^{2\Omega t} - 1) + \frac{1}{2\alpha}, \quad D = \frac{\nu}{4\Omega}(1 - e^{-2\Omega t}) + \frac{1}{2\alpha}. \quad (58)$$

As $t \rightarrow 0$, $C \rightarrow \frac{1}{2\alpha}$, $D \rightarrow \frac{1}{2\alpha}$, and Eq. (57) recovers Eq. (53). For $t \neq 0$, C and D depend on the relative magnitude of $4\nu/\Omega$ and $1/2\alpha$.

Before proceeding to random α , we note that for a constant value of α , Eq. (57) shows the anisotropic distortion and decay of the profile of vorticity fluctuation by shear flows. The time evolution of $\omega(\mathbf{x}, t)$ for constant $\alpha = 100$ is shown in Fig. 5, where time $t = 0, 0.5, 1, 1.5$ increases from left to right. Of notable is the flattening and elongation of $\omega(x, y, t)$ along $z_1 = x + y = 0$, with the formation of a sheet like structure. This is quite similar to what is seen in Fig. 4, recalling that a narrow \mathbf{k} profile corresponds to a broad \mathbf{x} profile.

When $\alpha (> 0)$ is random, the statistics of $\omega(\mathbf{x}, t)$ depends on α as

$$p(\omega, \mathbf{x}, t) = \left| \frac{d\alpha}{d\omega} \right| p(\alpha). \quad (59)$$

In particular, at $t = 0$, Eq. (53) gives $\alpha = -4 \ln(\omega(t = 0)) / r^2$, where $r^2 = x^2 + y^2$, leading to

$$p(\omega, \mathbf{x}, 0) = \frac{4}{\omega r^2} p(\alpha). \quad (60)$$

For our purpose, it suffices to assume that α is uniformly distributed within a certain range. Two cases of our interest are the limit of weak inhomogeneity, where (i) $\alpha = [0, \frac{2\Omega}{\nu} e^{-2\Omega t}]$ and of a strong inhomogeneity and (ii) $\alpha = [\frac{2\Omega}{\nu}, \alpha_c]$ with $\alpha_c > \frac{2\Omega}{\nu}$. In case (i), the shearing does not have much influence on the scale of inhomogeneity, while in case (ii), it does have a significant effect. Starting our analysis in case (i), we approximate $C \sim D \sim \frac{1}{2\alpha}$, and consequently

$$\omega(\mathbf{x}, t) \sim \exp \left[-\frac{\alpha}{4} (e^{2\Omega t} z_1^2 + e^{-2\Omega t} z_2^2) \right] = \exp \left[-\frac{\alpha}{4} G_1 \right], \quad (61)$$

where $G_1 = e^{2\Omega t} z_1^2 + e^{-2\Omega t} z_2^2$. Eqs. (59) and (61) will then give us

$$p(\omega, \mathbf{x}, t) = \frac{2\nu}{\omega \Omega (z_1^2 + e^{-4\Omega t} z_2^2)}, \quad (62)$$

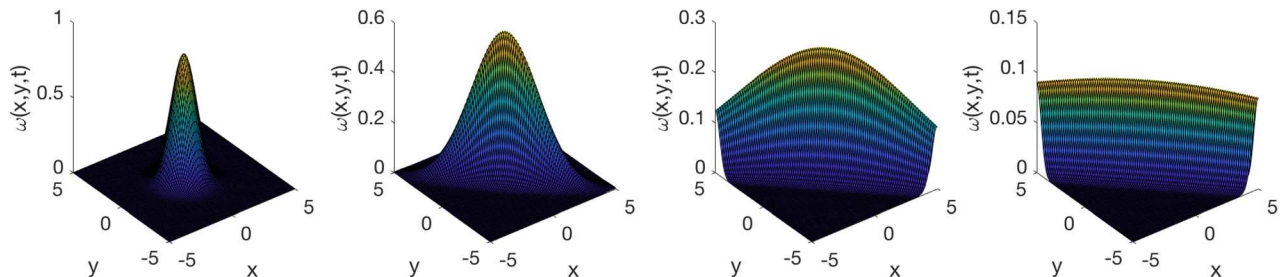


FIG. 5. Time evolution of $\omega(x, y, t)$ for $\Omega_z = \Omega_x = \Omega = 2$, $t = 0, 0.5, 1, 1.5$ increasing from left to right; $\alpha = 2$, $\nu = 0.1$, and $\phi = 1$.

for $\alpha < \frac{2\Omega}{\nu} e^{-2\Omega t}$. In Eq. (62), we used $p(\alpha) = \frac{\nu e^{2\Omega t}}{2\Omega}$ for $\alpha = [0, \frac{2\Omega}{\nu} e^{-2\Omega t}]$. A rapid decrease of $p(\omega, \mathbf{x}, t)$ in Eq. (62) for large z_1^2 is similar to the elongation of the vorticity profile along z_2 , observed in Fig. 5. We note here that the condition on $\alpha < \frac{2\Omega}{\nu} e^{-2\Omega t}$ is translated into $\omega(\mathbf{x}, t) > \exp[-\frac{\Omega G_1}{2\nu} e^{-2\Omega t}] \sim \exp[-\frac{\Omega}{2\nu} (z_1^2 + e^{-4\Omega t} z_2^2)]$.

The case (ii) where $\alpha = [\frac{2\Omega}{\nu}, \alpha_c]$, we have $\omega(\mathbf{x}, t) \sim \frac{2\Omega}{\alpha\nu} e^{-\Omega t - G_2}$, where $G_2 = \frac{\Omega}{2\nu} (z_1^2 + e^{-2\Omega t} z_2^2)$. Thus,

$$p(\omega, \mathbf{x}, t) \propto \frac{2\Omega}{\alpha\nu\omega^2} e^{-\Omega t - G_2}, \quad (63)$$

for $\omega = [\frac{2\Omega}{\nu} e^{-\Omega t - G_2}, e^{-\Omega t - G_2}]$, becoming very small for large z_1^2 . Compared with Eq. (60) or (62), $p(\omega, \mathbf{x}, t) \propto \omega^{-2}$ in Eq. (63) drops more rapidly for large ω . Interestingly, this is similar to the narrowing of Gaussian PDFs by shear flows shown in Sec. IV. Finally, going back to our discussion on the PDF method in Sec. II, we can compute the first three terms in Eq. (5) using our $p(\omega, \mathbf{x}, t)$ above to realize that a correct form of the last term in Eq. (5) is quite complicated and non-linear in $p(\omega, \mathbf{x}, t)$, as noted in Sec. II. The diffusion term in Eq. (1) cannot be simply neglected and needs to be treated very carefully.

VI. DISCUSSION AND CONCLUSIONS

We have presented the first analytical study of the effects of shear flows on enhanced dissipation in a decaying turbulence in 2D by incorporating the effects of shear flows non-perturbatively. We considered different initial power spectra and shear flows (ZF, ZF+ST) and clearly demonstrated how shear flows induce the rapid formation of small scales (large wave number modes), significantly enhancing the dissipation of turbulence. We presented time-dependent PDFs and discussed the effects of enhanced dissipation by shear flows on PDFs and effective dissipation time scale τ_e . While previous works advocated a hybrid time scale $\tau_e \propto \Omega^{-2/3} \tau_\eta$ (e.g., Ref. 16), where τ_η is the time scale due to a molecular diffusion, we showed that the dependence of τ_e on Ω (Ω_z) varies with initial power spectra and also types of shear flows. In addition, we demonstrated the utility of a dynamical time scale $\tau(t)$ in understanding the effect of shears, which quantifies the rate of the change in information (the rate at which a system passes through statistically different states).

Overall, τ_e and $\tau(t)$ tend to be much smaller for an initial δ -function power spectrum and for hyperbolic ZF+ST. ZF

can dramatically reduce $\tau(t)$ for an initial δ -function power spectrum but not for a constant power spectrum. This was however obtained in the case where the mean vorticity $\langle\omega_T\rangle$ is independent of time.³⁵ A time-varying $\langle\omega_T\rangle = -\Omega_z$, which is more likely in real situations (e.g., time-varying zonal flows), would however make $\tau(t)$ very small (see [Appendix C](#)), with interesting consequences to be investigated. Finally, hyperbolic ZF+ST was shown to cause an exponential increase in wavenumber, with a double exponential decrease in $\langle\omega^2\rangle$.

The preferential dissipation by shear flows in a certain direction can lead to a strongly anisotropic turbulence, as also shown in Refs. 7–9 (with a possibility of the reduction in dimension), in analogy to the maintenance of a 2D flow in a forced 3D rotating turbulence.³⁶ In 3D, the vortex stretching (which is absent in 2D) could somewhat compensate the severe quenching of vorticity amplitude. However, for a linear shear flow $\mathbf{U} = -x\Omega\hat{y}$, Eq. (D14) in [Appendix D](#) (see also Ref. 8) shows that the Fourier components of the velocity damp in time as $\tilde{v}_x \propto t^{-2}e^{-\nu Q(t,0)}$, $\tilde{v}_z \propto e^{-\nu Q(t,0)}$, and $\tilde{v}_y \propto e^{-\nu Q(t,0)}$ to leading order for $t > \frac{k_x(0)}{k_y\Omega}$. Here, $Q(t,0) = \frac{1}{3}(k_y\Omega)^2 t^3 + k_y k_x(0)\Omega t^2 + [k_x(0)^2 + k_y^2 + k_z^2]t$. Therefore, in addition to the enhanced dissipation $e^{-\nu Q(t,0)}$ through the time-dependent wave number, v_x undergoes the additional algebraic ($\propto t^{-2}$) quenching. The vorticity fluctuation $\tilde{\omega}$ would then be at most $\propto t e^{-\nu Q(t,0)}$ in y and z directions. Investigation of the effect of different shear flows on 3D turbulence, the extension to different models such as interchange turbulence,³⁴ magnetic dissipation, and dynamos, and implications for extreme events³⁷ are left for future work.

APPENDIX A: RELATION BETWEEN \mathcal{L} AND RELATIVE ENTROPY

We first show the relation between $\tau(t)$ in Eq. (10) and the second derivative of the relative entropy (or Kullback-Leibler divergence) $D(p_1, p_2) = \int dx p_2 \ln(p_2/p_1)$, where $p_1 = p(x, t_1)$ and $p_2 = p(x, t_2)$ as follows:

$$\frac{\partial}{\partial t_1} D(p_1, p_2) = - \int dx p_2 \frac{\partial_{t_1} p_1}{p_1}, \quad (\text{A1})$$

$$\frac{\partial^2}{\partial t_1^2} D(p_1, p_2) = \int dx p_2 \left[\frac{(\partial_{t_1} p_1)^2}{p_1^2} - \frac{\partial_{t_1}^2 p_1}{p_1} \right], \quad (\text{A2})$$

$$\frac{\partial}{\partial t_2} D(p_1, p_2) = \int dx [\partial_{t_2} p_2 + \partial_{t_2} p_2 (\ln p_2 - \ln p_1)], \quad (\text{A3})$$

$$\frac{\partial^2}{\partial t_2^2} D(p_1, p_2) = \int dx \left[\partial_{t_2}^2 p_2 + \frac{(\partial_{t_2} p_2)^2}{p_2} + \partial_{t_2}^2 p_2 (\ln p_2 - \ln p_1) \right]. \quad (\text{A4})$$

By taking the limit where $t_2 \rightarrow t_1 = t$ ($p_2 \rightarrow p_1 = p$) and by using the total probability conservation (e.g., $\int dx \partial_t p = 0$), Eqs. (D3) and (D5) lead to

$$\lim_{t_2 \rightarrow t_1 = t} \frac{\partial}{\partial t_1} D(p_1, p_2) = \lim_{t_2 \rightarrow t_1 = t} \frac{\partial}{\partial t_2} D(p_1, p_2) = \int dx \partial_t p = 0,$$

while Eqs. (D4) and (D6) give

$$\lim_{t_2 \rightarrow t_1 = t} \frac{\partial^2}{\partial t_1^2} D(p_1, p_2) = \lim_{t_2 \rightarrow t_1 = t} \frac{\partial^2}{\partial t_2^2} D(p_1, p_2) = \int dx \frac{(\partial_t p)^2}{p}.$$

To link this to information length \mathcal{L} , we then express $D(p_1, p_2)$ for small $dt = t_2 - t_1$ as

$$D(p_1, p_2) = \left[\int dx \frac{(\partial_{t_1} p(x, t_1))^2}{p} \right] (dt)^2 + O((dt)^3), \quad (\text{A5})$$

where $O((dt)^3)$ is a higher order term in dt . We define the infinitesimal distance (information length) $dl(t_1)$ between t_1 and $t_1 + dt$ by

$$dl(t_1) = \sqrt{D(p_1, p_2)} = \sqrt{\int dx \frac{(\partial_t p)^2}{p} dt + O((dt)^{3/2})}. \quad (\text{A6})$$

The total change in information between time 0 and t is then obtained by summing over $dl(t_1)$ and then taking the limit of $dt \rightarrow 0$ as

$$\begin{aligned} \mathcal{L}(t) &= \lim_{dt \rightarrow 0} [dl(0) + dl(dt) + dl(2dt) + dl(3dt) + \dots + dl(t-dt)] \\ &= \lim_{dt \rightarrow 0} \left[\sqrt{D(p(x, 0), p(x, dt))} + \sqrt{D(p(x, dt), p(x, 2dt))} \right. \\ &\quad \left. + \dots + \sqrt{D(p(x, t-dt), p(x, t))} \right] \\ &\propto \int_0^t dt_1 \sqrt{\int dx \frac{(\partial_{t_1} p)^2}{p}}. \end{aligned} \quad (\text{A7})$$

APPENDIX B: ANISOTROPIC CONSTANT POWER SPECTRUM

To demonstrate an incoherent shearing effect in the presence of multiple modes, it is interesting to consider an isotropic power spectrum by keeping a constant spectrum in k_y but taking $k_x(0) \sim 0$. The mean square vorticity is obtained from Eq. (31) by taking $k_x(0) \rightarrow 0$, with the result

$$\langle\omega^2(x, t)\rangle = \sqrt{\frac{\pi}{2\nu t \left(1 + \frac{1}{3}\Omega_z^2 t^2\right)}} \phi. \quad (\text{B1})$$

Thus, $\langle\omega^2(x, t)\rangle \propto t^{-3/2}$, decreasing less rapidly than $\langle\omega^2(x, t)\rangle \propto t^{-2}$ in Eq. (31). On the other hand, the effective dissipation time τ_e is similar to Eq. (32).

APPENDIX C: SLOWLY TIME-VARYING ZF

We assume $\Omega_z = \Omega_{z0} e^{-t/\tau_0}$ and $k_{x0} \sim 0$. Then, we have

$$k_x(t) = \int_0^t dt_1 k_y \Omega_z(t_1) = k_y \Omega_{z0} \tau_0 (1 - e^{-t/\tau_0}), \quad (\text{C1})$$

$$\begin{aligned} Q_1(t) &= (k_y \Omega_{z0} \tau_0)^2 \frac{\tau_0}{3} [1 - e^{-t/\tau_0}]^3 + k_y^2 t \\ &\sim \frac{1}{3} (k_y \Omega_{z0})^2 \tau_0^3 + k_y^2 t, \end{aligned} \quad (\text{C2})$$

$$\partial_t \Omega_z \sim -\frac{1}{\tau_0} \Omega_{z0}, \quad (\text{C3})$$

for $t \ll \tau_0$. Thus, Eqs. (12), (31), and (33) with the help of Eqs. (C2) and (C3) give us

$$\begin{aligned} \mathcal{E} &= \frac{1}{\tau(t)^2} = \frac{1}{2} \frac{(\partial_t \beta)^2}{\beta^2} + 2\beta (\partial_t \Omega_z)^2 \\ &\sim \frac{\left(4 + \frac{2}{3} \Omega_z t^2\right)^2}{2t^2 \left(4 + \frac{1}{3} \Omega_z t^2\right)^2} + \frac{2\nu t \sqrt{4 + \frac{1}{3} \Omega_z t^2}}{\pi \phi \tau_0^2} \Omega_{z0}^2. \end{aligned} \quad (\text{C4})$$

The second term is due to the change of Ω_z measured in the unit of the very small PDF width $\propto \beta^{-\frac{1}{2}} \propto \langle \omega^2 \rangle^{\frac{1}{2}}$. As time increases, the second term obviously makes a significant contribution.

APPENDIX D: 3D HYDRODYNAMIC TURBULENCE

In 3 D, the main governing equations for the total velocity $\mathbf{u} = \mathbf{v} + \mathbf{U}$ are⁸

$$\partial_t \mathbf{u} + \mathbf{u} \cdot \nabla \mathbf{u} = -\nabla p + \nu \nabla^2 \mathbf{u} + \mathbf{f}, \quad (\text{D1})$$

$$\nabla \cdot \mathbf{u} = 0, \quad (\text{D2})$$

where \mathbf{f} is a small scale forcing in general. By using $\mathbf{U} = -x\Omega\hat{y}$,

$$\partial_t \hat{v}_x = -ik_x \hat{p} + \hat{f}_x, \quad (\text{D3})$$

$$\partial_t \hat{v}_y - \Omega \hat{v}_x = -ik_y \hat{p} + \hat{f}_y, \quad (\text{D4})$$

$$\partial_t \hat{v}_z = -ik_z \hat{p} + \hat{f}_z, \quad (\text{D5})$$

$$0 = k_x \hat{v}_x + k_y \hat{v}_y + k_z \hat{v}_z, \quad (\text{D6})$$

where the second term in Eq. (D4) is due to the vortex stretching. Here, \hat{w} and \tilde{w} for $w = v_i, p$, and f are defined as

$$w(\mathbf{x}, t) = \tilde{w}(\mathbf{k}, t) \exp\{i(k_x(t)x + k_y y + k_z z)\}, \quad (\text{D7})$$

$$\hat{w} \equiv \tilde{w} \exp\{\nu(k_x^3/3k_y \Omega + k_H^2 t)\}, \quad (\text{D8})$$

where $k_H^2 = k_y^2 + k_z^2$; $k_x(t) = k_x(0) + \Omega k_y t$. Now, to solve coupled equations (D3)–(D6), we introduce a new time variable $\tau = k_x/k_y + \Omega t$ and rewrite them as

$$\Omega \partial_\tau \hat{v}_x = -i\tau k_y \hat{p} + \hat{f}_x, \quad (\text{D9})$$

$$\Omega \partial_\tau \hat{v}_y - \Omega \hat{v}_x = -ik_y \hat{p} + \hat{f}_y, \quad (\text{D10})$$

$$\Omega \partial_\tau \hat{v}_z = -ik_z \hat{p} + \hat{f}_z, \quad (\text{D11})$$

$$0 = \tau \hat{v}_x + k_y \hat{v}_y + \frac{k_z}{k_y} \hat{v}_z. \quad (\text{D12})$$

A straightforward, but rather long, algebra then gives us the solutions in the following form:

$$\begin{aligned} \hat{v}_x(\tau) &= \frac{1}{\gamma + \tau^2} \int^\tau d\tau_1 h_1(\tau_1), \\ \hat{v}_z(\tau) &= \int^\tau d\tau_1 \left[\frac{\tilde{\beta}}{\tau_1} \hat{v}_x - \frac{\tilde{\beta}}{\tau_1} \hat{f}_x + \hat{f}_z \right], \\ &= -\frac{\tilde{\beta}\tau}{\gamma} \hat{v}_x + \int^\tau d\tau_1 \frac{1}{\gamma} \\ &\quad \times \left[h_2(\tau_1) - \frac{\tilde{\beta}}{\gamma^{1/2}} \left(\tan^{-1} \frac{\tau}{\sqrt{\gamma}} - \tan^{-1} \frac{\tau_1}{\sqrt{\gamma}} \right) h_1(\tau_1) \right], \\ \hat{v}_y(\tau) &= -\tau \hat{v}_x(\tau) - \tilde{\beta} u \hat{v}_z(\tau), \\ \hat{p} &= \frac{\Omega}{k_y} (-\partial_\tau \hat{v}_x + \hat{f}_x), \end{aligned} \quad (\text{D13})$$

where $\tilde{\beta} = k_z/k_y$, $\gamma = 1 + \tilde{\beta}^2$, $h_1 = (1 + \tilde{\beta}^2) \hat{f}_x - \tau \hat{f}_y - \tau \tilde{\beta} \hat{f}_z$, and $h_2 = -\tilde{\beta} \hat{f}_y + \hat{f}_z$. Finally, going back to the original variable $k_x = k_y \tau$, we obtain

$$\begin{aligned} \tilde{v}_x(\mathbf{k}(t), t) &= \int dt_1 d^3 k_1 \frac{k_y^2}{k^2} \hat{g}(\mathbf{k}, t; \mathbf{k}_1, t_1) e^{-\nu Q(t, t_1)} \tilde{h}_1(\mathbf{k}_1, x, t_1), \\ \tilde{v}_z(\mathbf{k}(t), t) &= -\frac{k_x k_z}{k_H^2} \tilde{v}_x(\mathbf{k}(t), t) + \int dt_1 d^3 k_1 \hat{g}(\mathbf{k}, t; \mathbf{k}_1, t_1) \\ &\quad \times e^{-\nu Q(t, t_1)} \tilde{h}_2(\mathbf{k}_1, x, t_1) \\ &\quad \times \left[\frac{k_y^2}{k_H^2} \tilde{h}_2(\mathbf{k}_1, x, t_1) - \frac{k_z k_y^2}{|k_H^3|} \right. \\ &\quad \times \left. \left[\tan^{-1} \left(\frac{k_x}{|k_H|} \right) - \tan^{-1} \left(\frac{k_{1x}}{|k_{1H}|} \right) \right] \tilde{h}_1(\mathbf{k}_1, x, t_1) \right], \\ \tilde{v}_y(\mathbf{k}(t), t) &= -\frac{k_x}{k_y} \tilde{v}_x(\mathbf{k}(t), t) - \frac{k_z}{k_y} \tilde{v}_z(\mathbf{k}(t), t). \end{aligned} \quad (\text{D14})$$

Here, $Q(t, t_1) = \int_{t_1}^t dt' [k_x^2(t') + k_H^2] = [k_x^3 - k_{1x}^3]/3k_y \Omega + k_H^2 (t - t_1)$; $k_H^2 = k_y^2 + k_z^2$; $k^2 = k_H^2 + k_x^2$; $\hat{g}(\mathbf{k}, t; \mathbf{k}_1, t_1) = \delta(k_y - k_{1y}) \delta(k_z - k_{1z}) \delta[k_x - k_{1x} - k_{1y} (t - t_1) \Omega]$; $\tilde{h}_1 = (1 + k_z^2/k_y^2) \tilde{f}_x - k_x \tilde{f}_y/k_y - k_x k_z \tilde{f}_z/k_y^2$; $\tilde{h}_2 = -k_z \tilde{f}_y/k_y + \tilde{f}_z$. By taking $\tilde{f}_i(t_1) = \tilde{v}_i(t_1) \delta(t_1)$, we obtain the homogeneous solution without the forcing.

¹K. H. Burrell, *Phys. Plasmas* **4**, 1499 (1997).

²T. S. Hahm, *Plasma Phys. Controlled Fusion* **44**, A87 (2002); **1**, 2940 (1994); **2**, 1648 (1995).

³M. Dam, M. Brons, J. J. Rasmussen, V. Naulin, and J. S. Hesthaven, *Phys. Plasmas* **24**, 022310 (2017).

⁴C. S. Chang, S. Ku, G. R. Tynan, R. Hager, R. M. Churchill, I. Cziegler, M. Greenwald, A. E. Hubbard, and J. W. Hughes, *Phys. Rev. Lett.* **118**, 175001 (2017).

⁵E. Kim and P. H. Diamond, *Phys. Rev. Lett.* **91**, 075001 (2003); E. Kim, *Mod. Phys. Lett. B* **18**, 551 (2004).

⁶E. Kim, *Phys. Rev. Lett.* **96**, 084504 (2006); E. Kim and B. Dubrulle, *Phys. Plasmas* **8**, 813 (2001).

⁷E. Kim, *Astron. Astrophys.* **441**, 663 (2005).

⁸E. Kim and N. Leprovost, *Astron. Astrophys.* **456**, 617 (2006); N. Leprovost and E. Kim, *Astron. Astrophys. Lett.* **463**, L9 (2007); E. Kim and N. Leprovost, *Astron. Astrophys.* **465**, 633 (2007); N. Leprovost and E. Kim, *Astron. Astrophys.* **468**, 1025 (2007).

⁹E. Kim, *Phys. Plasmas* **12**, 090902 (2005); E. Kim, *Phys. Plasmas* **13**, 022308 (2006); E. Kim and P. H. Diamond, *Phys. Plasmas* **11**, L77 (2004).

¹⁰J. Li and Y. Kishimoto, *Phys. Plasmas* **11**, 1493 (2004).

¹¹Y. Idomura, S. Tokuda, and Y. Kishimoto, *Nucl. Fusion* **45**, 1571 (2005).

¹²X. U. Guosheng and W. U. Xingquan, *Plasma Sci. Technol.* **19**, 033001 (2017).

- ¹³E. J. Synakowski, S. H. Batha, M. A. Beer, M. G. Bell *et al.*, *Phys. Plasmas* **4**, 1736 (1997).
- ¹⁴X. Garbet, *Plasma Phys. Controlled Fusion* **43**, A251 (2001).
- ¹⁵G. Rewoldt, M. A. Beer, M. S. Chance, T. S. Hahm *et al.*, *Phys. Plasmas* **5**, 1815 (1998).
- ¹⁶P. H. Diamond, S.-I. Itoh, K. Itoh, and T. S. Hahm, *Plasmas Phys. Controlled Fusion* **47**, R35 (2005); P. H. Diamond, A. Hasegawa, and K. Mima, *ibid.* **53**, 124001 (2011).
- ¹⁷M. E. McIntyre, *J. Atmos. Terr. Phys.* **51**, 29 (1989).
- ¹⁸J. C. R. Hunt and P. A. Durbin, *Fluid Dyn. Res.* **24**, 375 (1999).
- ¹⁹A. Sood, E. Kim, and R. Hollerbach, *J. Phys. A: Math. Theor.* **49**, 425501 (2016).
- ²⁰A. P. Newton and E. Kim, *Phys. Plasmas* **18**, 052305 (2011).
- ²¹S. B. Pope, *Turbulent Flows* (Cambridge University Press, 2000).
- ²²J. Zinn-Justin, *Quantum Field Theory and Critical Phenomena* (Clarendon Press, 2002).
- ²³H. Risken, *The Fokker-Planck Equation: Methods of Solution and Applications* (Springer, Berlin, 1996).
- ²⁴S. B. Nicholson and E. Kim, *Phys. Lett. A* **379**, 83–88 (2015).
- ²⁵S. B. Nicholson and E. Kim, *Entropy* **18**, 258 (2016).
- ²⁶J. Heseltine and E. Kim, *J. Phys. A: Math. Theor.* **49**, 175002 (2016).
- ²⁷E. Kim, U. Lee, J. Heseltine, and R. Hollerbach, *Phys. Rev. E* **93**, 062127 (2016).
- ²⁸E. Kim and R. Hollerbach, *Phys. Rev. E* **95**, 022137 (2017).
- ²⁹R. Hollerbach and E. Kim, *Entropy* **19**(6), 268 (2017).
- ³⁰B. R. Frieden, *Physics from Fisher Information* (Cambridge University Press, Cambridge, 2000).
- ³¹W. K. Wootters, *Phys. Rev. D* **23**, 357 (1981).
- ³²G. Ruppeiner, *Phys. Rev. A* **20**, 1608 (1979).
- ³³F. Schlögl, *Z. Phys. B - Cond. Matt.* **59**, 449 (1985).
- ³⁴I. Movahedi and E. Kim, “Effects of shear flows on the evolution of fluctuations in interchange turbulence,” *Phys. Plasmas* (to be published); [arXiv:1711.04897](https://arxiv.org/abs/1711.04897).
- ³⁵In such a case, $\tau(t)$ essentially measures the rate of change in the differential entropy $\propto -\int dx p \ln p = \frac{1}{2} [1 - \ln(\frac{\beta}{\pi})]$ for a Gaussian PDF in Eq. (11).
- ³⁶B. Gallet, *J. Fluid Mech.* **783**, 412 (2015).
- ³⁷E.-W. Saw, D. Kuzzay, D. Faranda, A. Guittonneau, F. Daviaud, C. Wiertel-Gasquet, V. Padilla, and B. Dubrulle, *Nat. Commun.* **7**, 12466 (2017).